HOSTED BY

ELSEVIER

CrossMark

Available online at www.sciencedirect.com

ScienceDirect

Journal of Magnesium and Alloys 2 (2014) 342−348
www.elsevier.com/journals/journal-of-magnesium-and-alloys/2213-9567

Full length article

Effects of casting process on microstructures and flow stress behavior of Mg−9Gd−3Y−1.5Zn−0.8Zr semi-continuous casting billets

Xuan liu, Qichi Le*, Zhiqiang Zhang, Lei Bao, Zhengxing Fan, Jianzhong Cui

Key Lab of Electromagnetic Processing of Materials, Ministry of Education, Northeastern University, 314Mailbox, Shenyang 110819, People's Republic of China

Received 18 September 2014; revised 18 November 2014; accepted 19 November 2014
Available online 8 December 2014

Abstract

Mg−9Gd−3Y−1.5Zn−0.8Zr alloys own high strength, good heat and corrosion resistance. However, it is difficult for the fabrication of large-scale billets, due to the poor deformation ability and strong hot-crack tendency. This work investigated the casting process on the microstructures and flow stress behaviors of the semi-continuous casting billets for the fabrication of large-scale Mg−9Gd−3Y−1.5Zn−0.8Zr billets. The casting process (electromagnetic intensity and casting speed) shows outstanding effects on the microstructures and flow stress behavior of the billets. The billets with the specific casting process (I = 68 A, V = 65 mm/min) exhibit uniform microstructures and good deformation uniformity.

Keywords: Mg−Gd−Y−Zn−Zr; Semi-continuous casting; Microstructures; Flow stress behavior

1. Introduction

Recently, the lightening of materials has become a spot for research, due to the energy and resource limitation. Magnesium alloys become one of the most attractive metallic materials because of their low density, high specific stiffness and good damping capacity [1]. However, the poor mechanical properties frustrate magnesium alloys' applications.

As we know, magnesium alloys with RE additions could enhance the mechanical properties drastically, especially at elevated temperatures. It is reported that Mg−Gd−Y−Zr alloys exhibit the higher specific strength at both room temperature and elevated temperatures. Meanwhile, they own more excellent creep resistance than WE54 [2,3]. Thus, it provides an effective approach to improve the strength of Mg alloys. Recently, a $Mg_{97}Zn_1Y_2$ with excellent tensile yield strength above 600 MPa were manufactured through rapidly solidified powder metallurgy [4]. It should be attributed to the fine grains and distribution of long period stacking order phases (LPSO). It was reported that the LPSO phases showed outstanding effects on the mechanical properties of Mg−Gd−Y−Zn−Zr alloys [5−10]. Meanwhile, a research has been developed about the effect of Zn addition on the aging hardening of Mg−2.0Gd−1.2Y−0.2Zr (at. %) [11]. As a result, Mg−Gd−Y−Zn−Zr alloys could be the potential candidate to broaden the application of magnesium alloys.

However, the fabrication of Mg−Gd−Y−Zn−Zr alloys was not widely reported. Although the fabrication of Mg−8.2Gd−3.8Y−1.0Zn−0.4Zr has been achieved by semi-continuous casting [12], it is still rarely covered that external field like electromagnet (EM) was introduced during the semi-continuous casting of Mg−Gd−Y−Zn−Zr alloys. Low-frequency electromagnetic casting (LFEC) has been applied in the semi-continuous casting of Al−Zn−Mg−Cu−Zr alloys

* Corresponding author. Tel.: +86 24 83683312; fax: +86 24 83681758.
E-mail address: qichil@mail.neu.edu.cn (Q. Le).

Peer review under responsibility of National Engineering Research Center for Magnesium Alloys of China, Chongqing University.

http://dx.doi.org/10.1016/j.jma.2014.11.007.

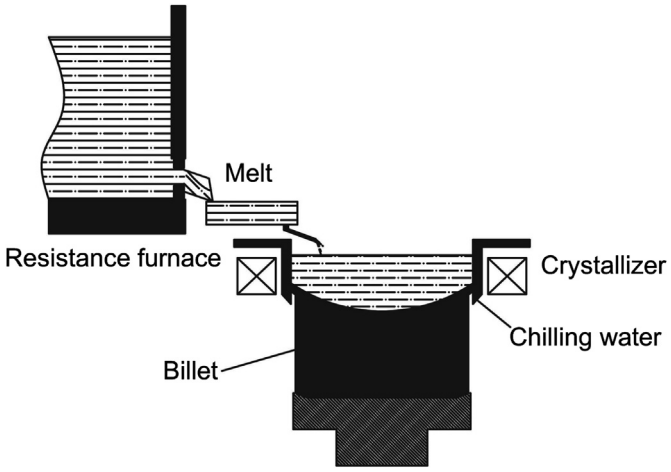

Fig. 1. Schematic for the casting process.

[13], which could restrain the macrosegregation and uniform the structure [14].

In this work, Mg–9Gd–3Y–1.5Zn–0.6Zr alloys are fabricated under electromagnetic field by semi-continuous casting. Investigations were carried out around the effects of casting speed and electromagnetic intensity on the microstructures of the alloys. Meanwhile, flow stress behavior will be also discussed.

2. Experimental

An alloy of chemical composition Mg–9.3Gd–3.2Y–1.5Zn–0.8Zr (wt. %) was prepared from high-purity (99.9%) Mg and Zn, Mg–25Gd (wt. %), Mg–50Y (wt. %) and Mg–30Zr (wt. %) master alloys by melting in resistance furnace and casting with a hot-top crystallizer under a shielding gas of mixed CO_2 and SF_6 at 690 °C. Fig. 1 shows the schematic for the casting process and casting apparatus are set as shown in Table 1. The billets have approximately a diameter of 190 mm and length of about 1000 mm, as shown in Fig. 2.

Fig. 2. The photo of the billet fabricated by semi-continuous casting.

Table 1
Casting parameters in this study.

Casting parameters		
Frequency of EM (Hz)	Intensity of EM (A)	Casting speed (mm/min)
30	68	55
30	68	65
30	90	65
0	0	65

The samples for the microstructure observation were cut from the center, 1/2 radius and near the surface of the alloy billets along axial and radial directions. The microstructures were etched in 4% Nital and observed using optical microscope (OM). Linear intercept method was applied to determine the grain size of the alloys. Flow stress behaviors were studied on a Gleeble-1500D thermal mechanical simulator in the temperature 400 and 450 °C, at constant strain rates of 0.1 s^{-1} and 1 s^{-1}. In addition, the Gleeble samples were 15 mm in diameter and 8 mm in height.

3. Results and discussion

3.1. Surface quality of the billets

Fig. 3 shows the surface qualities of billets. Structures of the hot-top crystallizer make severe influence on the surface of billets. Obvious lengthways streaks (Fig. 3a) are observed on the surface of the billet, and the depth of them could reach as much as about 3 mm. It would drastically decrease the final yield of billets. As the hot-top mould is mainly made up of refractories with a rough skin (Rags and scratches spread along the inner wall of the mould), large friction force generate on the inner wall of the hot-top mould during semi-continuous casting. Consequently, it gives rise to the poor surface quality of the billets. Moreover, the melt adhered and solidified on the inner wall of the mould at the primary stage. Thus, the billet (Fig. 3b) has a cup-like tail.

3.2. Microstructures of the as-cast billets

Fig. 4 shows the microstructures of the as-cast samples from edge to center of the billets. The microstructures of the billets are mainly composed of α-Mg and large amount of discontinuous eutectic around the grain boundaries. EM treatment reduces the grain sizes distinction ranging from edge to center of the billets. Fig. 5 illustrates the grain sizes of the different positions with and without EM treatment. The billet without EM infliction owns a wide grain size distribution from edge to center. Grain size for the edge position is as small as 27 μm, while that for the center reaches as large as 58 μm. This should be ascribed to the large temperature gradient and variant cooling rate between the edge and center, during the semi-continuous casting process.

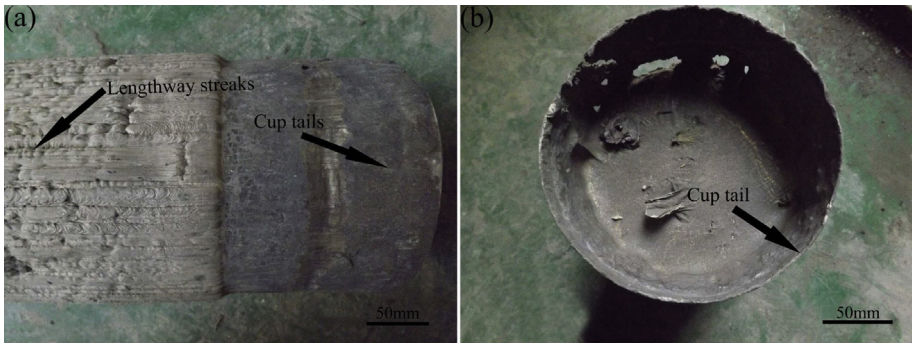

Fig. 3. Surface quality of the as-cast billets. (a) surface of the billets; (b) cup tail.

The microstructures of the billet become uniform after casting under an EM field ($f = 30$ Hz, $I = 68$ A), as shown in Fig. 4b, e and h. Grain size from edge to center are also uniform, as shown in Fig. 5. A forced convection in the liquid sump gives rise to the initial solidified grains detached following the induced liquid flow [15,16]. On the other hand, temperature gradient is also decreased by the induced convection, and it also make sense that the driving force bringing the overheated melt from the center to the periphery [17]. Moreover, the role of the hot top is also important. Its low heat convection coefficient ensures slow cooling of the melt from the edge in the initial stage of the cast. Consequently, the microstructures become uniform. While the EM treatment parameters change to $f = 30$ Hz, $I = 90$A, microstructures of the billet are refined apparently, as shown in Fig. 4c, f and i. Grain size from edge to center are also uniform. The average grain size are less than 30 μm, also shown in Fig. 5. It reveals that EM plays an important role on the solidified structure of the billets. The increasing of the current intensity enhances the force convection. Thus, electromagnetic stirring effect inhibits the grain growth efficiently. But 68 A is better than 90 A in the view of structure uniformity. What worth mentioning is that the grain size of the edge with EM ($I = 68$ A) is a bit larger than that without EM treatment. Interpretation should be given as the change of heat convection coefficient led by soft contact with the mold.

Fig. 6 shows the microstructures of the billets with different casting speeds. It can be seen that grains are more refined with a lower casting speed. That is because the liquid sump increases with the enlargement of the casting speed. Thus, the stirring effect made by EM is short and weak, and the temperature gradient is also increasing. As a result, the grains

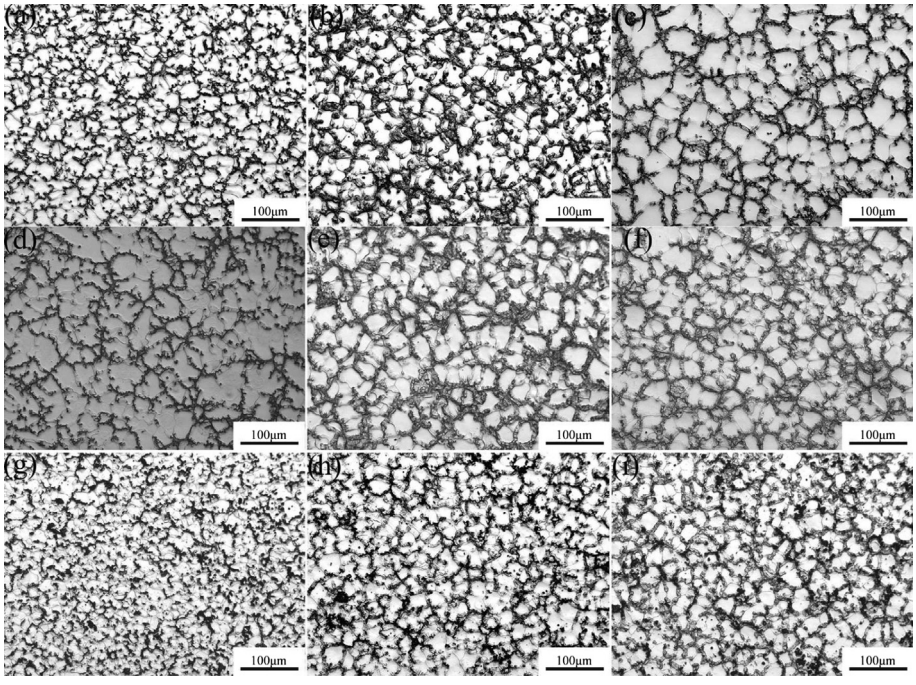

Fig. 4. Optical microstructures of the as-cast billets (from left to right: edge to center). (a), (b) and (c) without EM; (d), (e) and (f) with EM ($f = 30$ Hz, $I = 68$ A); (g), (h) and (i) with EM ($f = 30$ Hz, $I = 90$ A).

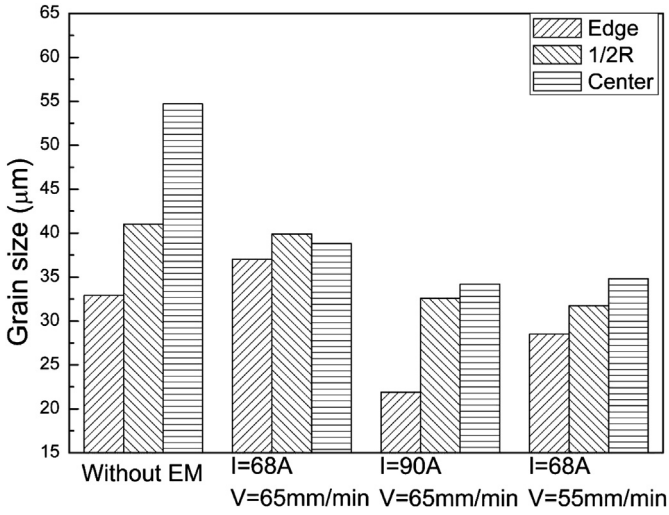

Fig. 5. As-cast alloy grain size of different electromagnetic conditions.

become coarser, and the structures of the billets could be refined with a low casting speed. Even so, microstructures become uniform with a casting speed of 65 mm/min, as shown in Fig. 5.

3.3. Flow stress of the as-cast alloy

In the previous chapter, the low frequent electromagnet could refine the microstructures of the billets. The different deformation ability between the edge and the center of the billets should be a key to the subsequent processes. Thus, the flow stress characters of the billets are now investigated to find the optimist casting parameters for the uniform deformation. Fig. 7 shows the true flow stress-true strain curves of the billets with different casting parameters. In general, low temperature and high strain rate will increase the flow stress, while higher temperature and lower strain rate will decrease the flow stress of the alloy [18]. This is due to the thermal activation processes that become intense by raising the deformation temperature.

Flow stress curves at 400 °C exhibit a sharp increase of the initial stage of strain and then slowly increase up to a transient equilibrium. When stress reaches the maximum value at, the stress decreases gradually and then drives to a steady value with the increasing strain, as shown in Fig. 7a, c, e and g. As the deformation temperature increases to 450 °C, flow stress behaviors become quite different. After the sharp increase on the stress, slow stress growth to the maximum value is missing as shown in Fig. 7b, d, f and h. Meanwhile, the flow stress behaviors are similar as the strain rate are 0.1 s^{-1} and 1 s^{-1}.

Fig. 8 shows the optical microstructures of samples with different strains at 400 °C. Large amount of lamellar phase are observed inside the grains. This lamellar phase should be identified as LPSO phase [11], which are formed during the hot compression process. From the microstructures of the sample with a strain of 0.1, some lamellar LPSO phase traverse the grains partially, while most of the LPSO run throughout the grains in the larger strained samples ($\varepsilon = 0.3$ and 0.6). Thus, it could be seen that the LPSO phases gradually run through the grains as the increasing strain. In other word, these lamellar phases play an important role on the flow stress behavior of the as-cast billets. It can be found that the flow stress curve is mainly composed of three stages: stage I (work hardening stage), stage II (softening stage) and stage III (steady stage) [19]. In the work hardening stage, the increasing number density of dislocations gives rise to the strong work hardening. On the other hand, the dynamic recovery is too weak to absorb the accumulating dislocations. Consequently, the flow stress quickly increases with the increase of strain. In the softening stage, the accumulated dislocation density exceeds the critical strain, giving rise to the formation of the lamellar LPSO phase. The nucleation and growth of LPSO phases need to absorb dislocations, which decreases the flow stress. In the short steady stage, the flow stress keeps a steady state due to the dynamic balance between the work hardening and dynamic softening. The nucleation and growth of LPSO phases is obviously significant to the soften stage.

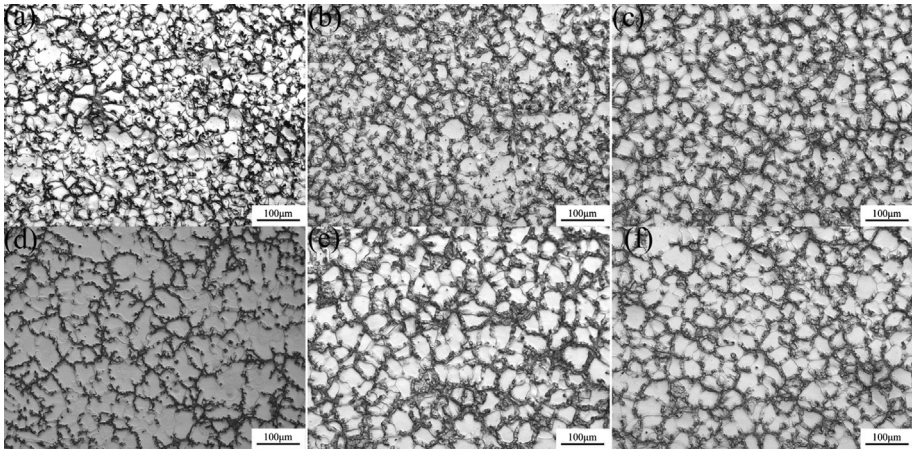

Fig. 6. Optical microstructures of the ingots from edge to center with different casting speeds (from left to right: edge to center). (a), (b) and (c) $v = 55$ mm/min; (d), (e) and (f) $v = 65$ mm/min.

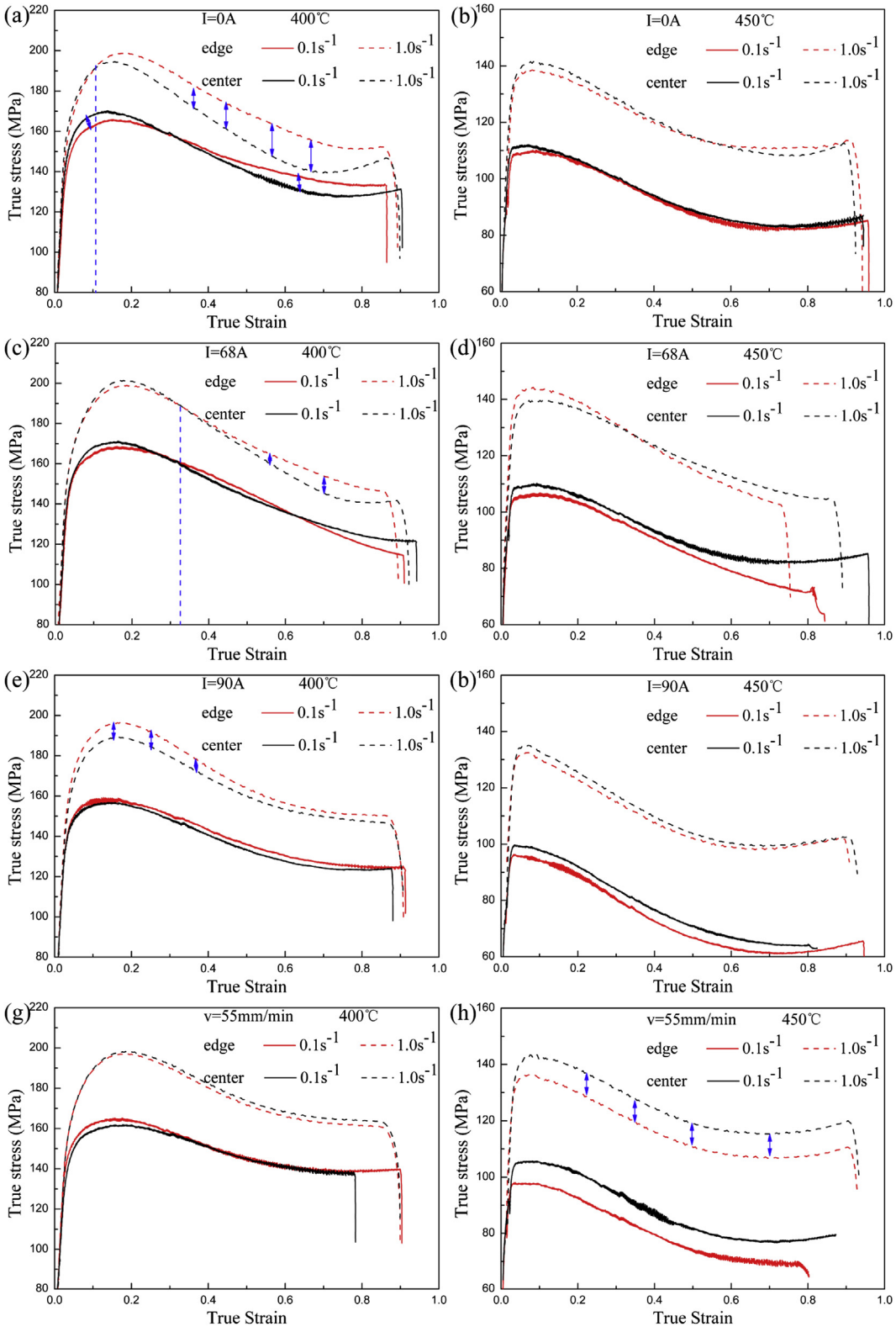

Fig. 7. True stress–strain curves of billets with different casting parameters.

From the flow stress curves in Fig. 7, it could be seen that billets with different casting process own distinct deformation uniformity. On condition that the strain rate is 1 s^{-1} and temperature is 400 °C, the flow stress difference between the edge and the center of the billet without EM is enlarged after the strain increases from 0.12 to 0.7, as shown in Fig. 7a, and similar situation occurs when the strain rate is 0.1 s^{-1}. Stress distinction between the edge and the center of the billet

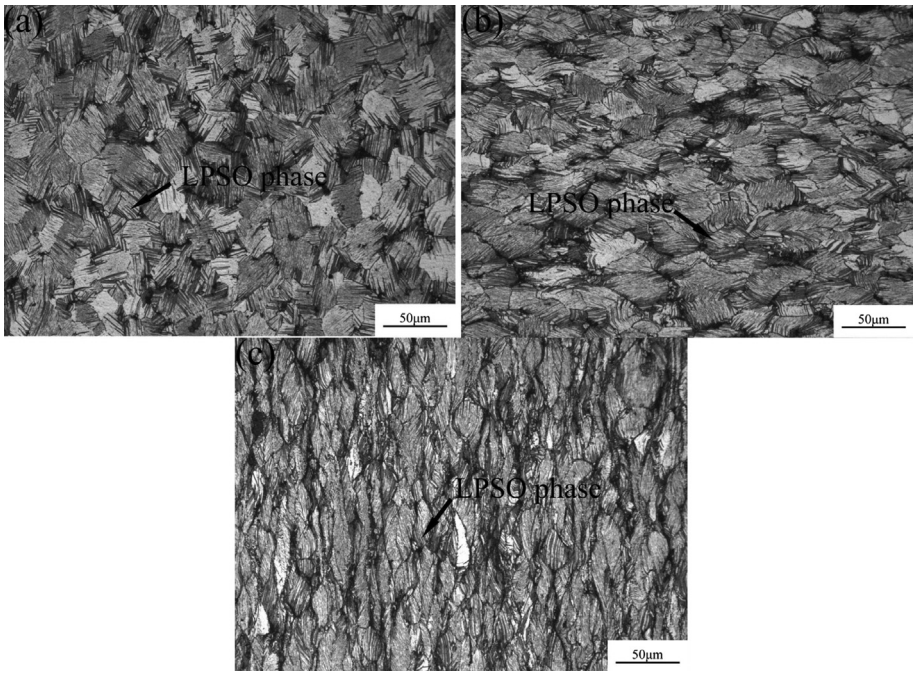

Fig. 8. The optical microstructures of compressed samples with different strains at 400 °C. (a) $\varepsilon = 0.1$; (b) $\varepsilon = 0.3$; (c) $\varepsilon = 0.6$.

(Fig. 7c) with EM ($I = 68$ A, $V = 65$ mm/min) is much smaller than that without EM. The difference is not enlarged until the strain increases to 0.36, when the strain rate is 1 s^{-1}. At a lower strain rate of 0.1 s^{-1}, flow stress curves are nearly synchronous for the edge and the center as the strain rises up. While the EM intensity increases to 90 A as shown in Fig. 7e, the flow stress difference is not narrowed further. It proves that large electromagnetic intensity could in turn do harm to the uniform deformation of the billets.

After deformation temperature rises up to 450 °C, EM intensity makes weak influence on the flow stress difference between the edge and the center of the billet. The higher temperature gives rise to the easier nucleation and growth of the lamellar LPSO phases. Thus, uniform deformation occurs at 450 °C.

Fig. 7 also shows the flow stress curves of billets with a casting speed of 55 mm/min. When deformation temperature is 400 °C and EM intensity is a constant of 68 A, the flow stress distinction between the edge and the center is very small as the strain increases. Moreover, the flow stress–strain curves of the edge and the center of the billet made by a casting speed of 55 mm/min is almost overlapped, as shown in Fig. 7g. It suggests a uniform deformation. When the casting speed increases to 65 mm/min and strain rate is 1 s^{-1}, the difference rises up after strain increases to 0.36, as shown in Fig. 7c. While the temperature increases to 450 °C, billet with a casting speed of 55 mm/min show a great difference in the flow stress between the edge and the center (Fig. 7h), however, it is better for the billet fabricated by a speed of 65 mm/min, as shown in Fig. 7d, and the flow stress difference (strain rate of 1 s^{-1}) is small when the strain is less than 0.34. It could be seen that the casting process shows an outstanding effect on the flow stress behavior of the billets in the viewpoint of deformation uniformity. Overall consideration, the billet with casting process ($I = 68$ A, $V = 65$ mm/min) shows the best deformation uniformity. Meanwhile, it also owns the largest maximum flow stress over others.

4. Conclusion

This work investigated the casting process on the microstructures and flow stress behaviors of the semi-continuous casting billets, aimed at the fabrication of large-scale Mg–9Gd–3Y–1.5Zn–0.8Zr billets. The casting process (electromagnetic intensity and casting speed) shows outstanding effects on the microstructures and flow stress behavior of the billets. The microstructures could be refined by increasing the electromagnetic intensity as well as decreasing the casting speed. The LPSO phase has outstanding effects on the flow stress behaviors of the alloy. Billets with proper EM intensity and casting speed own good deformation uniformity. The billets with the specific casting process ($I = 68$ A, $V = 65$ mm/min) exhibit uniform microstructures and good deformation uniformity.

Acknowledgment

This research was financially supported by National Basic Research Program of China (Grant No. 2013CB632203), the Liaoning Provincial Natural Science Foundation of China (Grant No. 201202072), National Key Technology R&D Program of China (2012BAF09B01), and the Fundamental Research Foundation of Central Universities (Grant Nos. N120509002 and N120309003).

References

[1] B. Smola, I. Stulıková, F. von Buch, B.L. Mordike, Mater. Sci. Eng. A 324 (2002) 113−117.
[2] I.A. Anyanwu, S. Kamado, Y. Kojima, Mater. Trans. 42 (2001) 1212−1218.
[3] X. Li, W. Qi, K. Zheng, N. Zhou, J. Magnesium Alloys 1 (2013) 54−63.
[4] Y. Kawamura, K. Hayashi, A. Inoue, T. Masumoto, Mater. Trans. 42 (2001) 1171−1174.
[5] C. Xu, M.Y. Zheng, K. Wu, E.D. Wang, G.H. Fan, S.W. Xu, S. Kamado, X.D. Liu, G.J. Wang, X.Y. Lv, Mater. Sci. Eng. A 559 (2013) 364−370.
[6] C. Xu, M.Y. Zheng, K. Wu, E.D. Wang, G.H. Fan, S.W. Xu, S. Kamado, X.D. Liu, G.J. Wang, X.Y. Lv, Mater. Sci. Eng. A 559 (2013) 615−622.
[7] C. Xu, M.Y. Zheng, K. Wu, E.D. Wang, G.H. Fan, S.W. Xu, S. Kamado, X.D. Liu, G.J. Wang, X.Y. Lv, M.J. Li, Y.T. Liu, Mater. Sci. Eng. A 559 (2013) 232−240.
[8] C. Xu, M.Y. Zheng, S.W. Xu, K. Wu, E.D. Wang, G.H. Fan, S. Kamado, X.D. Liu, G.J. Wang, X.Y. Lv, Mater. Sci. Eng. A 559 (2013) 844−851.
[9] C. Xu, M.Y. Zheng, S.W. Xu, K. Wu, E.D. Wang, S. Kamado, G.J. Wang, X.Y. Lv, Mater. Sci. Eng. A 547 (2012) 93−98.
[10] C. Xu, M.Y. Zheng, S.W. Xu, K. Wu, E.D. Wang, S. Kamado, G.J. Wang, X.Y. Lv, J. Alloys Compd. 528 (2012) 40−44.
[11] T. Honma, T. Ohkubo, S. Kamado, K. Hono, Acta Mater. 55 (2007) 4137−4150.
[12] C. Xu, M.Y. Zheng, Y.Q. Chi, X.J. Chen, K. Wu, E.D. Wang, G.H. Fan, P. Yang, G.J. Wang, X.Y. Lv, S.W. Xu, S. Kamado, Mater. Sci. Eng. A 549 (2012) 128−135.
[13] J. Dong, J. Cui, X. Zeng, W. Ding, Mater. Lett. 59 (2005) 1502−1506.
[14] B. Zhang, J. Cui, G. Lu, Mater. Lett. 57 (2003) 1707−1711.
[15] C. Vives, Metall. Trans. B 20 (1989) 623−629.
[16] C. Vives, Metall. Trans. B 20 (1989) 631−643.
[17] S. Guo, J. Cui, Q. Le, Z. Zhao, Mater. Lett. 59 (2005) 1841−1844.
[18] K. Zhang, M. Ma, X. Li, Y. Li, L. Liang, M. Bing, Rare Met. 30 (2011) 87−93.
[19] X.-M. Chen, Y.C. Lin, D.-X. Wen, J.-L. Zhang, M. He, Mater. Des. 57 (2014) 568−577.